

# Performance of Water-based Liquid Scintillator

D. Beznosko<sup>c</sup>, M.V. Diwan<sup>a</sup>, S.Hans<sup>b</sup>, D. Jaffe<sup>a</sup>, S.H. Kettell<sup>a</sup>, R.Rosero<sup>b</sup>,  
H. Themann<sup>a</sup>, B. Viren<sup>a</sup>, E. Worcester<sup>a</sup>, M. Yeh<sup>b</sup>, C. Zhang<sup>a</sup>

<sup>a</sup>*Physics Department, Brookhaven National Laboratory, Upton, NY 11973, USA*

<sup>b</sup>*Chemistry Department, Brookhaven National Laboratory, Upton, NY 11973, USA*

<sup>c</sup>*Department of Physics, Nazarbayev University, Astana, 010000, KZ*

---

## Abstract

The Water-based Liquid Scintillator (WbLS) is a new material currently under development. It is based on the idea of dissolving the organic scintillator in water using special surfactants. This material strives to achieve the novel detection techniques by combining the Cerenkov rings and scintillation light, as well as the total cost reduction compared to pure liquid scintillator (LS).

Presented are the light yield measurements for the three different proton beam energies (210MeV, 475MeV and 2000MeV) for water, two different WbLS formulations (0.4% and 0.99%) and pure LS. The results show that a goal of 100 optical photons/MeV, indicated by the simulation to be an optimal light yield for observing both the Cerenkov ring and scintillation light from the proton decay in a large water detector, has been achieved.

*Keywords:* Water based, liquid scintillator, beam test

---

## 1. Motivation

In large water detectors, the Cerenkov radiation produced by a charged particle above the threshold can be used for particle identification, and the reconstruction of its direction and energy [1]. However, all charged particles below the Cerenkov threshold are missed. Detecting these below-threshold particles is important for various applications. For example, in the search of the proton decay, in the  $p^+ \rightarrow K^+ \bar{\nu}$  channel, where  $K^+$  is mostly below Cerenkov threshold and is invisible in a water detector. The use of the WbLS

---

*Email address:* `dima@dozory.us` (D. Beznosko)

9 makes the kaon visible and allows for the separation of  $K^+$ ,  $\mu^+$  and  $e^+$  signals  
10 using timing and reduce background for this decay channel.

11 In either LS or WbLS, the isotropic scintillation light is produced by  
12 the charged particle energy deposition via ionization, but the scintillator  
13 components may interfere with the Cerenkov ring detection. To detect  $K^+$   
14 and preserve the Cerenkov ring, MC studies indicate that the light yield  
15 (LY) from the scintillator component in the WbLS should be 100 optical  
16 photons/MeV.

17 Thus, WbLS potentially combines both the Cerenkov ring and scintil-  
18 lation light capabilities. It can preserve the particle identification for the  
19 particles above the Cerenkov threshold, and detect the charged particles be-  
20 low the threshold via the scintillation light. In addition, WbLS features the  
21 lower cost than pure LS and it is safer to handle[ask Minfang for reference].

22 The ability to reach the desired LY can be checked using the mono-  
23 energetic proton beam with different WbLS concentrations. For the test,  
24 the two different WbLS formulations (0.4% and 0.99%), pure water and pure  
25 LS samples were chosen. Three different proton beam energies were used  
26 with each sample. The choice of the energies comes from the following con-  
27 siderations:

- 28 • 2000MeV protons behave as minimum ionizing particle (MIP)
- 29 • 475MeV protons are just below the Cerenkov limit in water
- 30 • 210MeV protons have  $\sim$ same energy deposition as  $K^+$  from the proton  
31 decay channel mentioned above.

## 32 2. Experimental Setup

33 The experimental setup used for the proton beam test is shown in (Fig-  
34 ure 1). Two tubs with the samples were used (T1 and T2). Three 2cm x  
35 2cm 5mm thick plastic scintillator hodoscopes were used (H1 to H3) with the  
36 beam trigger being formed by the coincidence of the H1&H2 only. H3 was  
37 intended to verify whether particles exit T2. .

### 38 2.1. Tub and Signal Readout Description

39 Two tubs were used in the experiment:

- 40 • T1 from Polytetrafluoroethylene (PTFE) (white, highly reflective),

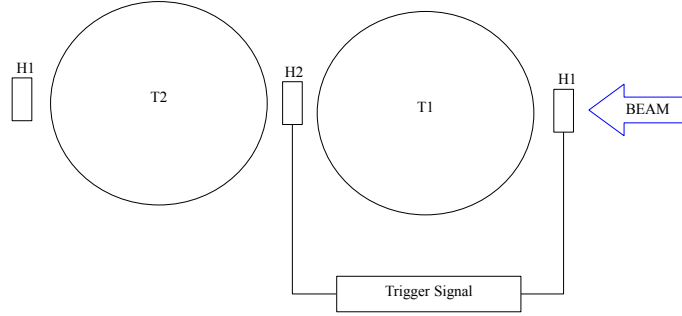


Figure 1: Proton beam test experimental setup.

- T2 from Aluminum, coated with black PTFE (very low reflectivity).

The T1 allows the capture of most of the light produced in the tub, whereas T2 allows for the observation of the light coming directly from the scintillation without the multiple wall reflections. An image of a tub is in (Figure 3). Both T1 and T2 have the same dimensions:

- the lid is 19.05mm thick,
- the walls and bottom are 6.35mm thick,
- inner height and diameter are 150mm.

. A detailed setup readout scheme is shown in (Figure 2). Both tubs were read out by Hamamatsu [2] R7723 2" Photo-multiplier tubes (PMT). An acrylic window transparent for the ultraviolet light (UVT) was used as a partition between the PMT and the liquid in the tub. The window was protruding through the lid and into the liquid by several millimeters to ensure that there are no air bubbles on its surface.

A readout was by the 4-channel 14bit CAEN [3] V1729A Flash Analog-to-Digital Converter (FADC). All tubs signals were connected to the FADC via a

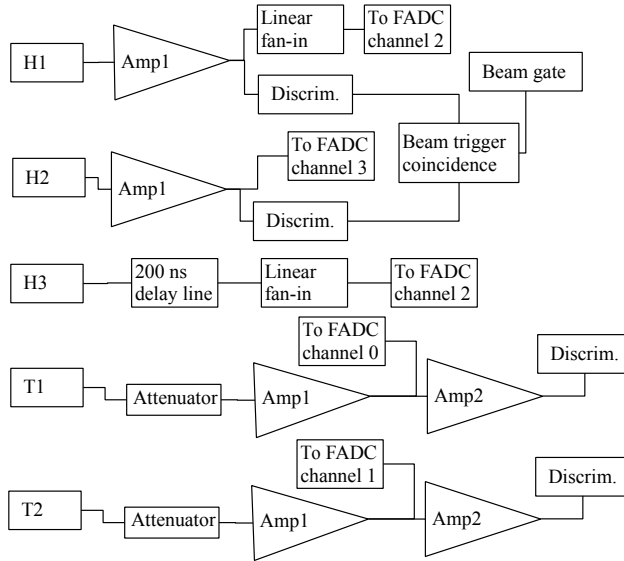


Figure 2: Proton beam test experimental setup.

variable attenuation unit (Phillips Scientific [4] 804) and a variable amplifier unit (Phillips Scientific 778). For the T1 and the T2 readouts, the gain was set to the values of  $\sim 2x$ . The first output from the amplifier goes to the FADC, with a dedicated channel for each tub. The second output from each amplifier channel was used for the single photo-electron (PE) calibration. The gain for the second amplification stage was set at  $\sim 10x$ .

All hodoscopes also were connected via  $\sim 2x$  gain amplifier channels that allows signal splitting. H1 and H3 shares the same FADC channel with latter signal being delayed by 200ns. H2 was connected to the last remaining channel of the FADC.

## 2.2. Triggering Scheme

Triggering schema was realized using three 2cm x 2cm, 5mm thick plastic scintillator counters that were readout by 2" PMTs via an air waveguide in order to remove the PMTs from direct beam exposure. The signal from the front-most and a middle counters were used to form a beam trigger, as indicated in the (Figure 2)

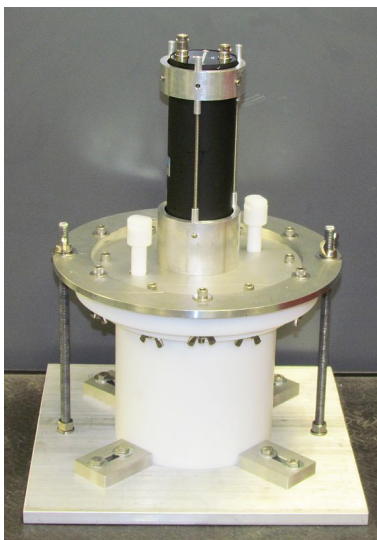


Figure 3: PTFE tub detector with a PMT.

### 2.3. Proton Beamline Description

A proton test beam was conducted at NASA Space Radiation Laboratory (NSRL) facility at BNL. As described above, the three proton beam energies were used: 210MeV, 475MeV and 2GeV. The beam had the following main characteristics:

- intensity of  $\sim 1p^+$ /bunch,
- beam size was 1cm x1cm at 2GeV and 5.4cm x 5.4cm at 210MeV,
- 0.4s long spills every  $\sim 4$  sec.

## 3. Data Analysis

### 3.1. Liquids Measured

???

4 samples tested: Water (purified) WbLS-1: 0.4WbLS-2: 0.99LS: 100

Water (purified) WbLS-1: 0.4WbLS-2: 0.99LS: LAB + 2g/L PPO + 15mg/L MSB.

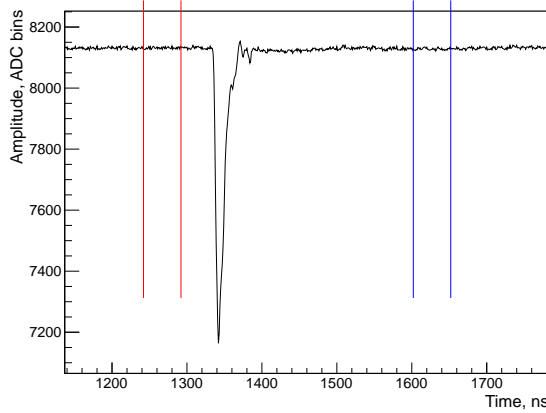


Figure 4: Typical PMT waveform with baseline check windows.

### 3.2. Waveform Analysis

The PMT signal is acquired as a waveform shown in (Figure 4). Total acquisition window is 2560 bins per event with each bin being 1ns wide; the signal is approximately centered and the approximate position is known beforehand. A 300ns window (central one in the figure, between the red and blue lines) is used to obtain the integrated signal area by summation. Each point is subtracted from the average baseline to achieve a positive sum. A typical signal is smaller than the chosen window width, however, there is a small spread in timing of the signals and we want to be sure that all of the signal has been integrated. The size of the chosen window is the same for all samples and measurements.

A baseline is defined as the average value of all the points in the first integration window (between the two red lines) that is 50ns wide. A typical baseline is shown in (Figure 5) To check the baseline quality, its averaged value is compared against the average of the post-signal window (between two blue lines). This difference is illustrated in (Figure 6). Events with this difference larger than  $\sim 20$  ADC bins are flagged as bad. This allows for the removal of the noise events or events with the bad baseline. Additionally, a comparison of the baseline with an average of a window at the very beginning of the waveform (between 10ns and 40ns, not shown because the figure is zoomed around the signal area) is used for general baseline quality check using the above criterion.

The integrated area is a measure of total charge that can be converted

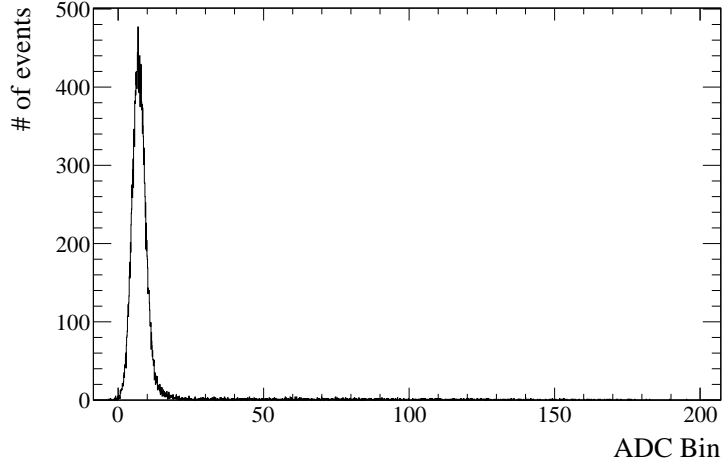


Figure 5: Typical baseline value for a single channel.

111 to the PE yield using the single PE calibration of the PMTs. This allows  
 112 to describe the measured signals independent of the hardware differences  
 113 between the channels.

114 The trigger information that is saved in the two additional FADC channels  
 115 allows for the offline trigger requirements be used.

### 116 3.3. Single Photo Electron Calibration

117 A single PE calibration was conducted for both signal channels at the end  
 118 of the test beam run. For it, the trigger is produced from the discriminator  
 119 that follows the second amplifier for the T1 and T2 signals (separately for  
 120 each, see Figure 2). The discriminator is set to  $\sim 1/10^{\text{th}}$  of the single PE  
 121 amplitude as to allows for better PE signal detection efficiency than using  
 122 random trigger. Additionally, this forces the PE signal to the signal window  
 123 region of the FADC output for the simplified analysis and elimination of the  
 124 partially captured signals. Note that a PE signal is much narrower and lower  
 125 in amplitude/area then the beam signals that are typically many PEs that  
 126 arrive with time distribution, thus a smaller integration window is used to  
 127 reduce noise for cleaner calibration (50ns instead of 300ns).

128 The signal area calibration is  $168.0 \pm 1.2$  ADC bins and  $132.9 \pm 1.6$  ADC  
 129 bins for T1 and T2 respectively (the PE signal is summed within the window,  
 130 so the unit of ADC bin is still used). A special care was taken to separately

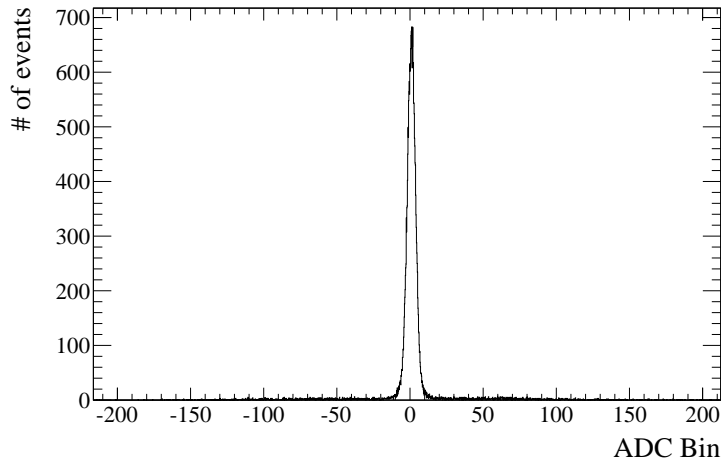


Figure 6: Difference between the baseline and the average of the post-signal window.

131 verify that this method yields the same calibration values as using the light-  
 132 emitting diode (LED) scheme. For that, calibration runs using the described  
 133 above scheme and using the dim LED pulses were compared to each other.  
 134 The LED light level is chosen such that only  $\sim 1/10^{\text{th}}$  of the events has the  
 135 single PE signal to insure that these are the single photon detection responses.

### 136 3.4. *Light Yield Analysis*

137 The analysis process involves establishing the data quality selection cri-  
 138 teria, data fitting, interpretation of the fitting results and the evaluation of  
 139 the systematic errors. Each step is included within this chapter.

#### 140 3.4.1. *Data quality selection*

141 The data quality selection is done as a single step before the data is  
 142 analyzed. The care was taken to choose the criteria that do not introduce a  
 143 bias into the selection. These are:

- 144 • offline double trigger requirement for H1 and H2 to be above  $\sim 50\text{mV}$   
 145 and within the expected time window,
- 146 • baseline quality check as outlines in chapter 3.2,
- 147 • ADC saturation check for H1 and H2.



Each check is intended to remove potential noise or multiple particles in an event. The saturation check indicates if several particles have passed through the hodoscopes in a same beam spill that happens rarely at the intensity used.

### 3.5. Light Yield Results

For each sample and energy, a histogram of the signal areas is computed. A fit using a Gaussian and a bin likelihood method is then performed. The fitting is done in two steps - first, a Gaussian is fitted in the range between the half of the maximum peak values to obtain the first approximation. Then, the fits around the found mean with  $1$ ,  $1.5$  and  $2\sigma$  are carried. This is done to estimate the uncertainty that the fit width is adding because of the second peak due to the two particles passing through the tub during the same trigger time. Figure 3.5 shows the  $1.5\sigma$  fit of the single particle fit, and the two-particle peak is visible on it as well. This plot is in the ADC bins for clarity; single-PE calibration will be applied to all further plots.

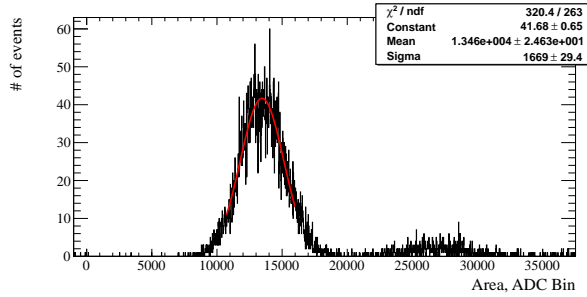


Figure 7: A sample fit of a tub signal.

The data for all the samples at all energies is then processed in the same way. Plots in Figure 3.5 and in Figure 3.5 show the light yield results in PE for the different samples and beam energies for Tub1 and tub2 respectively.

### 3.6. Energy deposition

In order to estimate the PE/MeV light yield of each sample, the energy deposition in each sample is needed. Two methods were used for this purpose: a GEANT4 simulation of the beamline setup with the deposition being the mean of the 1000runs at each energy, and a simplified code that would calculate the proton energy loss along a straight line path through the tubs

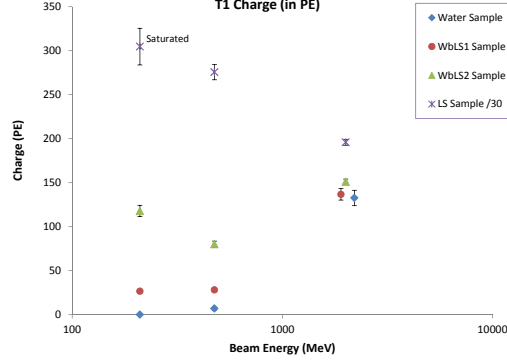


Figure 8: The light yield in PE for T1. At 2GeV beam energy, some points are offset for clarity.

172 and hodoscopes with small steps, using the proton stopping power and range  
 173 tables (PSTAR) from the National Institute of Standards and Technology  
 174 (NIST). The WbLS was modeled as water, and the LS as toluene.

175 The resulting energy depositions are listed in Table 1. The difference  
 176 between the two methods is taken as the uncertainty for the values obtained  
 177 (summed with RMS of the mean as square root of the sum of the squares).

Table 1: Energy Deposition in Samples

Beam Energy (MeV)	Sample	T1 Energy Deposit (MeV)	T2 Energy Deposit (MeV)
210	Water, WbLS	$72.7 \pm 3.1$	$107.5 \pm 6.1$
	LS	$59 \pm$	$124 \pm$
475	Water, WbLS	$40.4 \pm 2.0$	$43.7 \pm 2.2$
	LS	$34 \pm$	$36 \pm$
2000	Water, WbLS	$28.6 \pm 2.6$	$28.7 \pm 3.1$
	LS	$24 \pm$	$24 \pm$

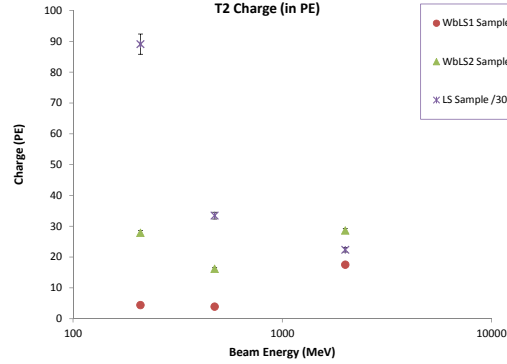


Figure 9: The light yield in PE for T2.

### 178 3.7. Systematics

#### 179 3.7.1. Calibration Stability

## 180 4. Conclusion

## 181 References

- 182 [1] M. Fechner et.al. (The Super-Kamiokande Collaboration), ‘Kinematic re-  
183 construction of atmospheric neutrino events in a large water Cherenkov  
184 detector with proton identification’, Phys. Rev. D 79 (2009) 112010,  
185 arXiv:0901.1645
- 186 [2] Hamamatsu Photonics, 314-5 Shimokanzo, Toyooka-village, Iwatagun,  
187 Shizuoka-ken, 438-0193 Japan; <http://www.hamamatsu.com>
- 188 [3] CAEN (Costruzioni Apparecchiature Elettroniche Nucleari S.p.A.), Via  
189 della Vetraria 11, 55049 Viareggio, Province of Lucca, Italy, 0584 388398.
- 190 [4] Phillips Scientific, 31 Industrial Ave. Suite 1, Mahwah, N.J. 07430